Holocene deglaciation of Prudhoe Dome, northwest Greenland

TITLE: 58/90 characters

Caleb K. Walcott-George[1], Nathan D. Brown[2], Jason P. Briner[1], Allie Balter-Kennedy[3], Nicolás E. Young[3], Tanner Kuhl[4], Elliot Moravec[4], Sridhar Anandakrishnan[5], Nathan T. Stevens[6], Benjamin Keisling[7], Rob DeConto[8], Vasileios Gkinis[9], Joseph A. MacGregor[10], Joerg M. Schaefer[3]

[1]Department of Geology, University at Buffalo, Buffalo, NY, 14260, USA
[2]Department of Earth and Environmental Sciences, University of Texas at Arlington, Arlington, TX, 76019, USA
[3]Lamont-Doherty Earth Observatory, Columbia University, Palisades, NY, 10964, USA
[4]NSF Ice Drilling Program, University of Wisconsin, Madison, WI, 53706, USA
[5]Department of Geosciences, Pennsylvania State University, University Park, PA, 16802, USA
[6]Pacific Northwest Seismic Network, University of Washington, Seattle, WA, 98195, USA
[7]Institute for Geophysics, University of Texas at Austin, Austin, TX, 78758, USA
[8]Department of Geoscience, University of Massachusetts, Amherst, MA, 01003, USA
[9]Centre for Ice and Climate, Niels Bohr Institute, University of Copenhagen, Copenhagen, 2100, DK
[10]Cryospheric Sciences Laboratory, NASA Goddard Space Flight Center, Greenbelt, MD, 20771, USA

ABSTRACT

Projections of future sea-level rise benefit from understanding the response of past ice sheets to interglacial warmth. Constraints on the extent of inland Greenland Ice Sheet (GrIS) recession during the Middle Holocene (~8 – 4 ka) are limited because geological records of a smaller-than-modern phase largely remain beneath the modern ice sheet. We drilled through 509 m of firn and ice at Prudhoe Dome (PD), northwest Greenland to obtain sub-ice material yielding direct evidence for the response of the NW GrIS to Holocene warmth. Our infrared stimulated luminescence measurements from sub-ice sediments indicates that the ground below the summit was exposed to sunlight at 7.1 ± 1.1 ka. This complete deglaciation of PD, coeval to reduced extent at other ice caps across Northern Greenland, is further supported by interglacial-only $\delta^{18}O$ values from the PD ice column as well as ice depth-age modeling. Our results point to a significant response of the

NW GrIS to early Holocene warming, estimated to be +3–5 °C from paleoclimate data. This range of summer temperatures is similar to projections of warming by 2100 CE.

ABSTRACT WORD COUNT: 178/200

INTRODUCTION

The Greenland Ice Sheet (GrIS) has waxed and waned over the Quaternary, nearly completely deglaciating at least once in the last 1.1 Myr[1]. Evaluating the response of the GrIS to past warming is necessary to predict the future response of the ice sheet and its contributions to sea level rise [2]. Existing reconstructions suggest the central and southern GrIS retreated to its minimum Holocene size between ~5 and ~3 ka before readvancing to its historical maximum at ~1850 CE and provide an important framework for evaluating GrIS response to the most recent warm period[3]. However, these studies usually provide loose constraints on ice sheet footprint during these minima, making it difficult to fully assess the response of the GrIS to Holocene warmth. Meanwhile, cosmogenic nuclide and luminescence dating of sub-ice materials retrieved from ice core drilling campaigns can provide direct constraints on when locations in Greenland's far interior were ice-free in the past, resulting in more precise depictions of ice sheet geometry[1,4]. These studies have spurred new drilling projects aiming to assess the magnitude of GrIS inland retreat during the Holocene and its reaction to Holocene warmth by collecting sub-ice sediments and bedrock from key locations around the margins of the GrIS that can provide constraints on past ice sheet extents[5,6]. We present new infrared stimulated luminescence (IRSL) measurements from sub-ice sediments below the summit of Prudhoe Dome (PD), $\delta^{18}O$ measurements of the overlying ice column, and simple one-dimensional (1-D) ice depth-age modeling to provide robust evidence that PD deglaciated during the Holocene.

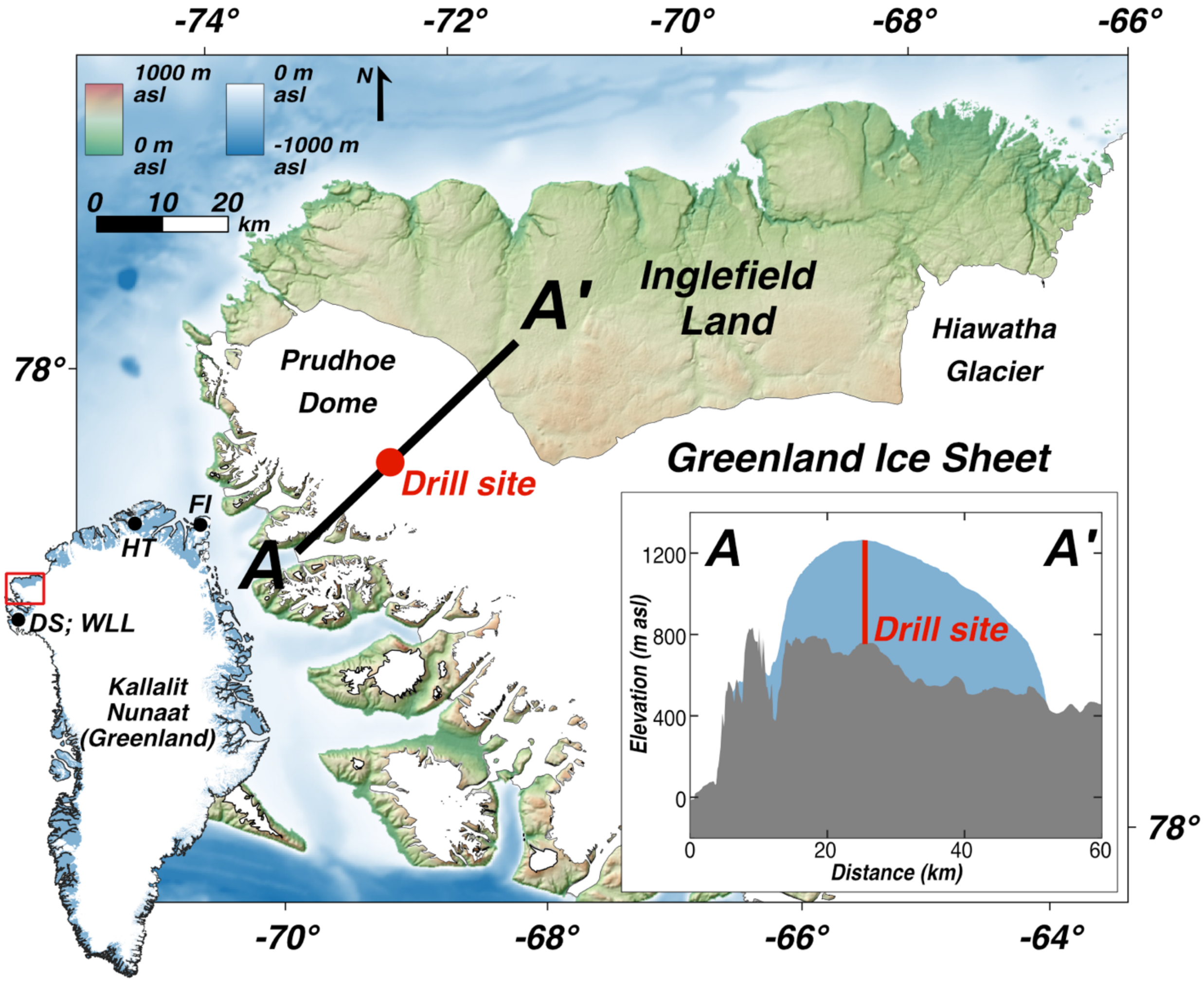

Figure 1: location of Prudhoe Dome in northwest Greenland showing drill site. Inset map of Greenland shows study area in red box and the locations of Hans Tausen (HT) and Flade Isblink (FI) ice caps, and Deltasø (DS) and Wax Lips (WLL) lakes. Inset cross-section shows ice thickness and bedrock topography of Prudhoe Dome measured by radar sounding [7] and the drill site.

Prudhoe Dome, northwest Greenland is a ~2500 km^2 ice dome with a maximum ice thickness of ~600 m attached to the main body of the GrIS via a saddle (Fig. 1). To its north and east, PD terminates at Inglefield Land, whereas its western and southern portions mostly terminate as marine outlet glaciers between narrow highlands. A recent synthesis of simulated GrIS basal thermal state indicates that the bed of PD is likely cold based[8]. Intensely weathered bedrock surfaces with high concentrations of cosmogenic nuclides suggest that the GrIS was mostly cold based when it covered Inglefield Land during the Quaternary[9]. During the Last Glacial Maximum (LGM; 26–19 ka), this sector of the GrIS expanded into Nares Strait, where it merged with the Innuitian Ice Sheet and flowed southward into northern Baffin Bay[10,11]. Ice retreated to the coast of modern-day Inglefield Land by ~9 ka, before reaching the present GrIS margin in central Inglefield Land at ~7 ka[12-15]. After ~7 ka, the GrIS continued to retreat to a smaller-than-modern position until it began readvancing to its Little Ice Age maximum[15]. The extent of the inland retreat of PD during the Holocene, and the timing of minimum extent, remains unknown. To assess this, we collected 3.0 m of sediment above 4.4 m of bedrock from a topographic high under 509.4 m of ice at the center of PD. We also retained ice chips from the ice column for $\delta^{18}O$ measurements.

The Holocene deglaciation of Prudhoe Dome

Luminescence ages from sediments record the duration since sediment grains were last exposed to sunlight. Minimum dose models of single-grain equivalent dose (D_e) derived from IRSL measurements on sand-sized K-feldspar in the upper 7.5 cm of the sub-ice sediments yield a burial age of 7.1 ± 1.1 ka (see methods). Our depth profile of D_e estimates reveals a sharp decrease of D_e towards the uppermost sediments; values at depth (~180 cm) of ~100 Gray (Gy) decrease to 14.4 ± 2.2 Gy at 0 – 2.5 cm (Fig 2B).

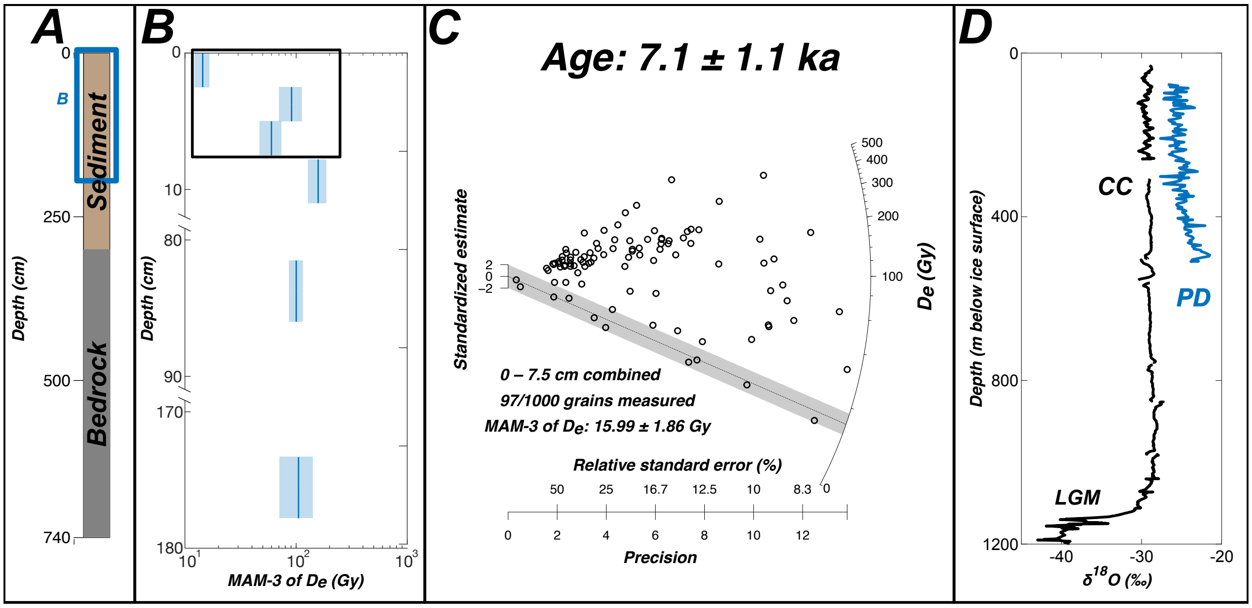

Figure 2:A) Simplified stratigraphic log of the ASIG core; blue box shows location of IRSL measurements in panel B. B) Minimum dose model (MAM3) of single-grain equivalent dose (D_e) with depth. Note breaks in y-axis. Blue line represents mean and transparent blue box represents the 1σ error. Black box shows upper 0-7.5 cm used to calculate burial age in panel C. C) Radial plot of single-grain K-feldspar measurements combined for grains (each grain measurement is an open circle) from 0 to 7.5 cm. Grey dashed line (mean) and grey transparent bar (1σ) shows MAM3 estimates of D_e. See Figure S1. for additional details on interpreting luminescence radial plots. Grains within the grey bar are represented by the pink grains in Fig. 3D, while grains outside the grey bar are represented by the red grains in Fig. 3D. D) $\delta^{18}O$ measurements from the overlying ice at our drill site (PD) measured every ~3 m, along with measurements from the Camp Century (CC) ice core [16].

At our site under the center of PD, exposure of sediment grains to sunlight occurs when PD is absent. Therefore, the burial age of our uppermost sediments of 7.1 ± 1.1 ka unambiguously requires PD to have deglaciated from our ice-dome summit drill site during the Holocene. Decreasing D_e values towards the surface are consistent with sediment mixing in the upper ~10 cm[17,18]. During sediment mixing (e.g., cryoturbation), fully bleached grains from the surface become mixed deeper into the sediment column and deeper grains are brought closer to the surface, where some become fully bleached (Fig. 3). Such mixing would occur until the site is buried by a glacier (e.g., the re-growth of PD), whereupon cryoturbation ceases, and the previously bleached sediment grains begin to record the burial duration. The skewed distribution of our D_e values with a population of low D_e grains among a larger population of higher D_e grains supports this hypothesis (Fig. 2B). We interpret our IRSL age from the upper 7.5 cm of sediment (7.1 ± 1.1 ka) as recording the cessation of sediment mixing and the initiation of Prudhoe Dome regrowth, thus serving as a minimum age for deglaciation and a maximum age for re-glaciation. Additionally, we observe no major decrease in $\delta^{18}O$ in PD ice, similar to that seen in the Camp Century ice core record at ~1050 m, representing Pleistocene ice (Fig. 2D). A lack of Pleistocene ice in the PD ice column is compatible with simple 1-D ice-age depth models of the ice column yield basal ice ages (Nye model: 3.4 to 7.9 ka; Extended Data Fig. 9)[19].

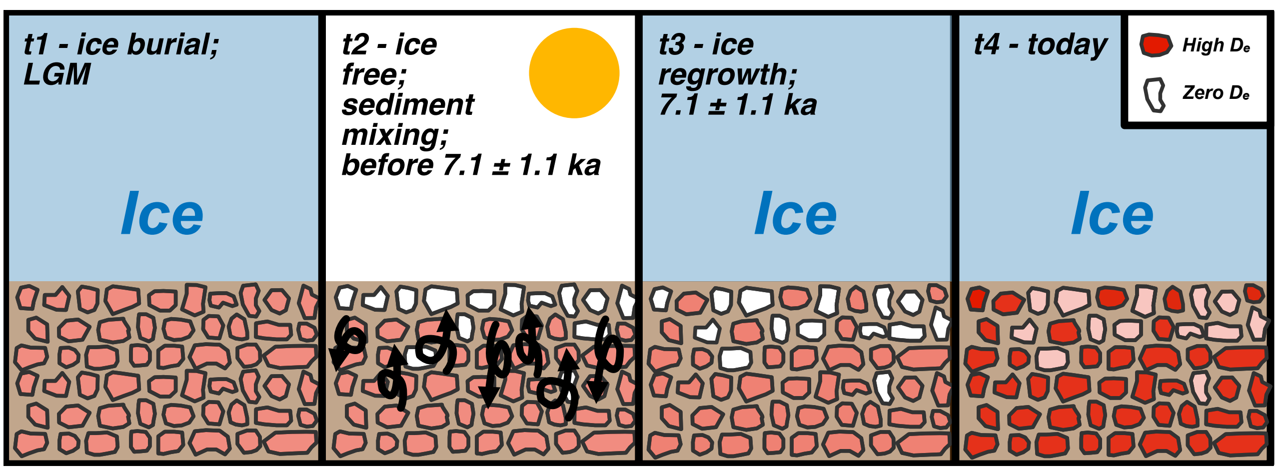

Figure 3: Conceptual model of luminescence resetting thorough sediment mixing during ice-free periods. t1) Sediments are buried beneath ice and each individual grain is accumulating a luminescence signal (red). t2) ice retreats, exposing the uppermost sediments to sunlight, resetting the luminescence signal. Sediment is mixed, bringing some grains with no luminescence signal lower in the column and some grains with preexisting luminescence signals towards the surface. t3) ice regrows over the sediment, cutting off sunlight. Sediments that saw sunlight prior to burial have no luminescence signal, while sediments that were not brought to the surface retain luminescence signals; sediment mixing has pooled together these grains with differing luminescence signals, where a minimum age model can identify the youngest population of grains (Fig. 2C). t4) sediment grains that saw sunlight during t2 record burial ages since ice regrowth (dots in grey bar in Fig. 2C). Sediment grains that did not see sunlight during t2 have luminescence that built up during multiple periods of ice burial (grains outside of grey bar in Fig. 2D)..

Because our drill site was located at the center of PD and above a topographic high, we infer that when our drill site became ice free, PD as an ice dome was largely, if not completely, absent. Post-LGM deglaciation at the modern coast of Inglefield Land, ~30 km north of PD, at ~9 ka is consistent with our IRSL age requiring PD absence before 7.1 ± 1.1 ka. A single *in-situ* ^{14}C age from a boulder at the ice edge ~40 km east of Prudhoe Dome records ice retreat near the modern margin there at 6.7 ± 0.3 ka[15]. This is broadly consistent with our IRSL age, though temporal differences in ice retreat may relate to glaciological differences between Prudhoe Dome and the main body of the northwestern GrIS.

The glacial history of North Greenland

The deglaciation of PD during the Holocene is compatible with other records of ice cap recession across northern Greenland (Fig. 4). A proglacial lake sediment record from Deltasø reveals that the North Ice Cap, ~180 km south of Prudhoe Dome, was smaller than present or absent from ~10.1 ka to 1850 CE[20]. An age–depth model based on evidence of known-age volcanic eruptions recorded in a 345-m-long ice core from Hans Tausen Ice Cap in northern Greenland suggest it completely deglaciated sometime during the Holocene and later regrew between 4.0 and 3.5 ka[21]. Proglacial threshold lake records show that Flade Isblink ice cap was smaller than present from ~9.4 to 0.2 ka, and that least parts of the ice cap may have persisted throughout the Holocene[22]. Ice-flow modeling and stable isotope measurements from an ice core suggest the main portion of Flade Isblink ice cap formed after 4.0 ka[23]. Across much of the Arctic, ice caps began to regrow by ~4 ka following their Holocene minima (Fig. 4)[24,25].

Reviews of existing GrIS-margin chronologies suggest that ice retreat behind the modern margin was spatially heterogeneous across Greenland, though it likely reached its minimum extent during the Middle Holocene (~5 – ~3 ka) and experienced several pronounced periods of Neoglaciation[3,26-28]. However, its exact geometry is unknown and there is likely substantial variability in the timing of that minimum extent across Greenland. In Inglefield Land, Hiawatha Glacier was smaller than today from >5.8 to <1.9 ka, while Humboldt Glacier retreated behind its present margin from sometime between >3.6 and <0.5 ka[15]. These records of ice cap and GrIS retreat suggest a complex pattern of ice sheet response to Holocene climate fluctuations.

Drivers of North Greenland deglaciation and regrowth

The deglaciation of PD broadly aligns with higher-than-modern Holocene temperatures reconstructed across other parts of Greenland between 10 and 4 ka, with large spatial variability[3,28]. Much of PD is land-terminating today and was likely completely land-terminating during Holocene deglaciation. Thus, retreat and ultimate complete deglaciation would not have been influenced by ice-ocean interactions such as calving and submarine melting but mostly governed by summer melt (surface mass balance). Summer temperatures reached their maximum in northwestern Greenland between ~10 and ~7 ka, as recorded by chironomid assemblages in lake sediment cores indicating July temperatures ~3 to 7 °C warmer than modern[20,25,29]. Similarly, a melt layer-derived summer temperature record from nearby Agassiz Ice Cap on Ellesmere Island reveal temperatures ~3 °C higher than modern between ~11 and 9 ka[30]. Meanwhile a coeval $\delta^{18}O$-based record of mean annual temperatures from Agassiz Ice Cap show ~3–6 °C of warming in the Early/Middle Holocene[30]. It appears that significant Early and Middle Holocene atmospheric warming drove increased surface melting to the point of completely melting PD.

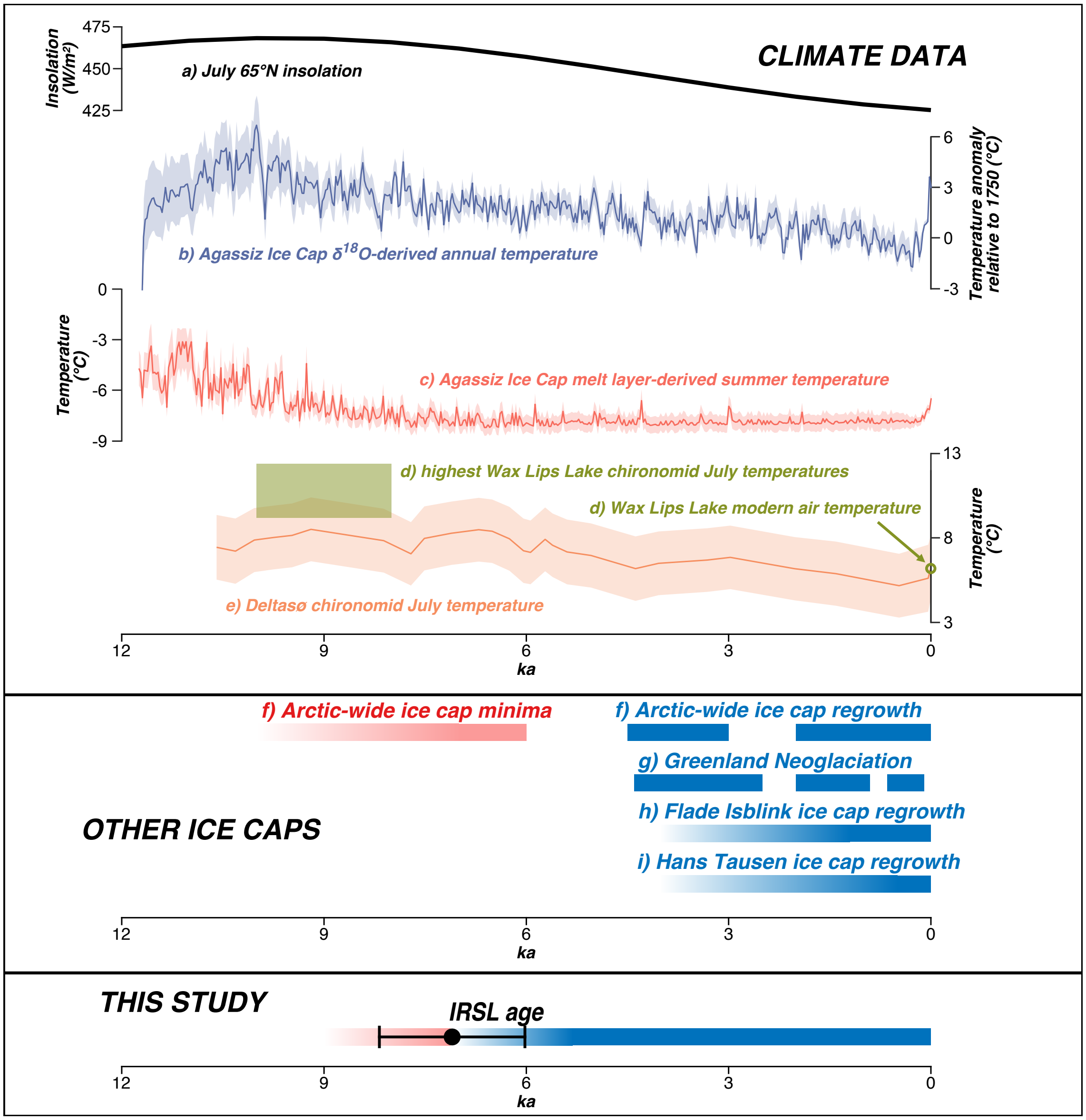

Figure 4: Regional paleoclimate data (a–d) compared against records of Arctic ice cap retreat/absence (red) and growth/presence (blue). Locations of Greenland records (d, g, h, and i) shown on Fig. 1. a) July insolation at 65°N [31], b) Agassiz Ice Cap annual $\delta^{18}O$ temperature record [30], c) Agassiz Ice Cap summer melt layer temperature record [30], d) chironomid July temperature estimates from Wax Lips Lake, NW Greenland, and modern Wax Lips Lake temperature[29] e) chironomid July temperature reconstructions from Deltasø, NW Greenland[20], f) summarized records of Arctic ice cap minima and re-growth[24],) g) summarized records of Greenland Ice Sheet Neoglaciation[28], h) record of Flade Isblink ice cap regrowth[23], i) record of Hans Tausen ice cap regrowth[21]. Black dot (mean) and error bars and (calculated by propagating D_e errors in quadrature) show IRSL burial age of the uppermost 7.5 cm from our sub-ice sediment core. Red bar shows period of PD deglaciation from modern coast of Inglefield Land[12-15] and blue shows regrowth/presence after deglaciation.

The full melt and regrowth of Prudhoe Dome during the Early-Middle Holocene points to an early and high amplitude summer warm anomaly in northwestern Greenland, as evidenced in paleoclimate records[24,25]. While a recent ice core synthesis indicates a near-uniform HTM onset by the mid-Holocene, our record from PD suggests an earlier summer HTM, with Holocene summer temperatures high enough to melt PD prior to 7.1 ± 1.1 ka[32]. Summer temperatures then had to decrease sufficiently to subsequently regrow PD within a few millennia, suggesting an early termination to summer HTM conditions paired with relatively steady precipitation through the Holocene[33]. However, given the differences in seasonality recorded in ice core records and the ablation-driven retreat of PD, a large increase in winter temperatures may perhaps obfuscate summer cooling, leading to a temporal mismatch between summer and annual HTM conditions[25,32]. Such large summer Holocene temperature changes in northwestern Greenland may implicate Arctic amplification (e.g., sea-ice feedbacks) in leading to higher amplitude Holocene summer temperature change in northern versus southern Greenland[3,25,34].

The magnitude of increased summer temperatures at the time of PD deglaciation are within the range of simulated 2100 CE summer warming at PD of between 1.8 and 4.7°C (CMIP5) and 2.4 and 5.7°C (CMIP6)[35]. Given the likelihood that CMIP projections underestimate the magnitude and rate of Arctic amplification (and therefore warming), summer temperatures at PD will likely reach levels that led to its Holocene deglaciation by 2100[36]. However, the duration required to deglaciate PD under these elevated temperatures remain unconstrained, suggesting that mitigation of future warming might ameliorate future melting of PD.

Luminescence analysis of sub-ice materials constrain the timing of minimum ice extent within the current GrIS footprint. Our IRSL age paired with $\delta^{18}O$ measurements and ice accumulation modeling unambiguously indicate the deglaciation and subsequent reglaciation of

Prudhoe Dome during the Early-Middle Holocene, pointing to a highly sensitive northern GrIS. This motivates future drilling efforts across the GrIS and peripheral ice caps to map the spatial pattern of inland retreat during the Holocene, offering additional insights into the evolution of the GrIS under elevated Arctic warming.

WORD COUNT: 1769/2200 excluding subheadings, figure captions, methods, acknowledgements, and methods

ACKNOWLEDGEMENTS

We thank the people and government of Kalaallit Nunaat (Greenland) for allowing us to conduct research on the island. Thank you to Richard Erickson, Forest Rubin Harmon, and the National Science Foundation Ice Drilling Program for drill operations, Jóhann Þorbjörnsson and Troy Nave for field support, Polar Field Services, especially Kyli Cosper, for field logistics, Kenn Borek Air, Air Greenland, and Matthias Vogt at Volcano Heli for flights, and Pituffik Space Base for pre- and post-field support. NSF grants 1933938 (University at Buffalo), 1933927 (Lamont-Doherty Earth Observatory), 1934477 (University of Massachusetts, Amherst), 1933802 (Pennsylvania State University) supported this research. JMS acknowledges support from the Vetlesen Foundation.

METHODS

Sub-ice drilling, ice, sediment, and bedrock collection

We used the Agile Sub-Ice Geologic (ASIG) drill operated by the NSF Ice Drilling Program to drill through PD and access the ice sheet bed at a geophysically-constrained topographic high (880 m asl) at the ice divide (1390 m asl). We collected ice chips from drill cuttings every ~3 m to for $\delta^{18}O$ measurements of the ice column. At 509.4 m ice depth, the drill encountered the ice-sheet bed upon which return fluid included sand grains along with the ice chips. We then collected a 7.5 m long core, comprising 3 m of frozen sediment on top of 4.5 m of gneissic bedrock. The upper 7.5 cm of the sediment core, drilled immediately after flushing the sediment-bearing cuttings, were kept in lightproof conditions for luminescence dating.

Luminescence dating

We sub-divided the light-shielded upper 7.5 cm into 3 segments at 2.5 cm intervals. We later sub-sampled inner portions of the core at 8.0–11.2 cm, 81.5–88.0 cm, and 167.9–173.2 cm under amber light at -20°C. We melted samples under amber light conditions at the University of Texas at Arlington Luminescence Lab (UTALL), where we used standard heavy liquids and acid treatment to isolate 150–200 µm potassium feldspar grains. We determined equivalent dose (D_e) values for individual K-feldspar grains from each depth interval using single-grain post-infrared infrared stimulated luminescence measured at 225°C (p-IR $IRSL_{225}$) [37]. We calculated cumulative D_e estimates for each depth interval and the combined measurements from 0–7.5 cm using a three-variable minimum age model (MAM3) assuming 15% overdispersion for single dose populations (Supplementary Table 1)[38]. We sent aliquots (1-10 g) of material from four depth intervals, 0-7.5 cm, 8.0–11.2 cm, 81.5–88.0 cm, and 173.3–177.8 cm, for XRF and ICP-MS measurements of radionuclides at SGS Canada (0-7.5 cm) or the Washington State University Peter Hooper GeoAnalytical Lab (8.0–11.2 cm, 81.5–88.0 cm, and 173.3–177.8 cm). We measured water content by measuring the mass of samples before melting and again after melting and after drying sediments in a 50 °C oven overnight. We calculated environmental dose rates for each segment of 2.5 cm from the upper 7.5 cm using alpha, beta, and gamma infinite matrix dose rates from DRAC, assuming inert overburden ice and a depth-dependent total dose rate field within the underlying sediment (Supplementary Tables 2, 3) [39,40]. To calculate the minimum age within the upper 7.5 cm, we used the average dose rate within this interval and the minimum dose model of all grains within this interval to calculate our burial age (Supplementary Table 4).

Oxygen isotope measurements

We collected ice chips following each drill run of 3 m, which constituted a mixture of ice chips from each run. We flushed the drill hole between each run to remove residual ice chips. We performed triple water-isotope analysis ($\delta^{17}O$, $\delta^{18}O$, δD) on drill ice chips using cavity ring-down spectroscopy (Picarro L-2140i) with a high-throughput vaporizer (Picarro A0212), following the protocol described in Gkinis et al. (2021), modified for drill chips. To prevent spectroscopic contamination from residual drill liquid, we incorporated a melt–refreeze step in the sample preparation procedure, allowing for the effective removal of organics. The sampling procedure provided a resolution of ~3 m.

Measurements are reported in permil (‰) relative to the Vienna Standard Mean Ocean Water and Standard Light Antarctic Precipitation (VSMOW–SLAP) international scale, defined by reference materials. We used three internal water standards with well-calibrated values against VSMOW–SLAP (Table water standards). The light and heavy standard materials (“-22” and “-

40") were used to construct a calibration curve, while the middle standard ("NEEM") served as a reference for accuracy estimation. Measurement precision was determined to be ±0.025‰ for $\delta^{17}O$, ±0.021‰ for $\delta^{18}O$, and ±0.23‰ for δD.

Ice depth-age modeling

We considered three one dimensional (1-D) steady-state ice-flow models to assess the depth–age relationship at our PD drill site (Fig. S9). More sophisticated transient, non-diffusive and three-dimensional modeling of the age of the GrIS has recently been demonstrated, but these models are presently too coarse (both spatially and temporally) to meaningfully resolve the age structure of the modern PD[41,42]. The three models are all conventionally applied for ice-sheet interiors[43], but here we calculate them analytically using a range of plausible Holocene and LGM conditions to aid first-order interpretation of our measured $\delta^{18}O$ drill ice chip record.

References (44/50)

1 Schaefer, J. M. *et al.* Greenland was nearly ice-free for extended periods during the Pleistocene. *Nature* **540**, 252-255 (2016). https://doi.org:https://doi.org/10.1038/nature20146

2 Briner, J. P. *et al.* Rate of mass loss from the Greenland Ice Sheet will exceed Holocene values this century. *Nature* **586**, 70-74 (2020). https://doi.org:https://doi.org/10.1038/s41586-020-2742-6

3 Briner, J. P. *et al.* Holocene climate change in Arctic Canada and Greenland. *Quaternary Science Reviews* **147**, 340-364 (2016). https://doi.org:https://doi.org/10.1016/j.quascirev.2016.02.010

4 Christ, A. J. *et al.* Deglaciation of northwestern Greenland during Marine Isotope Stage 11. *Science* **381**, 330-335 (2023). https://doi.org:10.1126/science.ade4248

5 Briner, J. P. *et al.* Drill-site selection for cosmogenic-nuclide exposure dating of the bed of the Greenland Ice Sheet. *The Cryosphere* **16**, 3933-3948 (2022). https://doi.org:10.5194/tc-16-3933-2022

6 Keisling, B. A. *et al.* An ice-sheet modelling framework for leveraging sub-ice drilling to assess sea level potential applied to Greenland. *EGUsphere* **2024**, 1-25 (2024). https://doi.org:10.5194/egusphere-2024-2427

7 CReSIS. (2024).

8 MacGregor, J. A. *et al.* GBaTSv2: a revised synthesis of the likely basal thermal state of the Greenland Ice Sheet. *The Cryosphere* **16**, 3033-3049 (2022). https://doi.org:10.5194/tc-16-3033-2022

9 Walcott-George, C. K., Balter-Kennedy, A., Briner, J. P., Schaefer, J. M. & Young, N. E. Glacial erosion and history of Inglefield Land, northwest Greenland. *EGUsphere* **2024**, 1-49 (2024). https://doi.org:10.5194/egusphere-2024-2983

10 Leger, T. P. M. *et al.* A Greenland-wide empirical reconstruction of paleo ice sheet retreat informed by ice extent markers: PaleoGrIS version 1.0. *Clim. Past* **20**, 701-755 (2024). https://doi.org:10.5194/cp-20-701-2024

11 Batchelor, C. L., Krawczyk, D. W., O'Brien, E. & Mulder, J. Shelf-break glaciation and an extensive ice shelf beyond northwest Greenland at the Last Glacial Maximum. *Marine Geology* **476**, 107375 (2024).

12 Mason, O. K. Beach ridge geomorphology at Cape Grinnell, northern Greenland: a less icy Arctic in the mid-Holocene. *Geografisk Tidsskrift-Danish Journal of Geography* **110**, 337-355 (2010). https://doi.org:https://doi.org/10.1080/00167223.2010.10669515

13 Nichols, R. L. Geomorphology of Inglefield land, north Greenland. *Meddelelser om Grønland* **188**, 3-105 (1969).

14 Blake, W., Boucherle, M. M., Fredskild, B., Janssens, J. A. & Smol, J. P. The geomorphological setting, glacial history and Holocene development of Kap Inglefield Sø, Inglefield Land, North-West Greenland. *Meddelelser om Grønland. Geoscience* **27**, 1-42 (1992).

15 Søndergaard, A. S. *et al.* Glacial history of Inglefield Land, north Greenland from combined in situ 10 Be and 14 C exposure dating. *Climate of the Past* **16**, 1999-2015 (2020). https://doi.org:https://doi.org/10.5194/cp-16-1999-2020

16 Johnsen, S. J., Dansgaard, W., Clausen, H. B. & Langway, C. C. Oxygen isotope profiles through the Antarctic and Greenland ice sheets. *Nature* **235**, 429-434 (1972).

17 Gray, H. J., Keen-Zebert, A., Furbish, D. J., Tucker, G. E. & Mahan, S. A. Depth-dependent soil mixing persists across climate zones. *Proceedings of the National Academy of Sciences* **117**, 8750-8756 (2020).

18 Reimann, T., Román-Sánchez, A., Vanwalleghem, T. & Wallinga, J. Getting a grip on soil reworking–Single-grain feldspar luminescence as a novel tool to quantify soil reworking rates. *Quaternary Geochronology* **42**, 1-14 (2017).

19 Nye, J. F. The distribution of stress and velocity in glaciers and ice-sheets. *Proceedings of the Royal Society of London. Series A. Mathematical and Physical Sciences* **239**, 113-133 (1957).

20 Axford, Y. *et al.* Holocene temperature history of northwest Greenland – With new ice cap constraints and chironomid assemblages from Deltasø. *Quaternary Science Reviews* **215**, 160-172 (2019). https://doi.org:https://doi.org/10.1016/j.quascirev.2019.05.011

21 Clausen, H. B. *et al.* Glaciological and chemical studies on ice cores from Hans Tausen Iskappe, Greenland. *Meddelelser Om Grønland. Geoscience* **39**, 123-149 (2001).

22 Larsen, N. K. *et al.* Local ice caps in Finderup land, north Greenland, survived the Holocene thermal maximum. *Boreas* **48**, 551-562 (2019).

23 Lemark, A. & Dahl-Jensen, D. A study of the Flade Isblink ice cap using a simple ice flow model. *Master's thesis, Niels Bohr Institute, Copenhagen University* (2010).

24 Larocca, L. J. & Axford, Y. Arctic glaciers and ice caps through the Holocene:a circumpolar synthesis of lake-based reconstructions. *Clim. Past* **18**, 579-606 (2022). https://doi.org:10.5194/cp-18-579-2022

25 Axford, Y., De Vernal, A. & Osterberg, E. C. Past warmth and its impacts during the Holocene thermal maximum in Greenland. *Annual Review of Earth and Planetary Sciences* **49**, 279-307 (2021).

26 Young, N. E. & Briner, J. P. Holocene evolution of the western Greenland Ice Sheet: Assessing geophysical ice-sheet models with geological reconstructions of ice-margin change. *Quaternary Science Reviews* **114**, 1-17 (2015). https://doi.org:https://doi.org/10.1016/j.quascirev.2015.01.018

27 Larsen, N. K. *et al.* The response of the southern Greenland ice sheet to the Holocene thermal maximum. *Geology* **43**, 291-294 (2015). https://doi.org:10.1130/G36476.1

28 Kjær, K. H. *et al.* Glacier response to the Little Ice Age during the Neoglacial cooling in Greenland. *Earth-Science Reviews* **227**, 103984 (2022). https://doi.org:https://doi.org/10.1016/j.earscirev.2022.103984

29 McFarlin, J. M. *et al.* Pronounced summer warming in northwest Greenland during the Holocene and Last Interglacial. *Proceedings of the National Academy of Sciences* **115**, 6357-6362 (2018).

30 Lecavalier, B. S. *et al.* High Arctic Holocene temperature record from the Agassiz ice cap and Greenland ice sheet evolution. *Proceedings of the National Academy of Sciences* **114**, 5952-5957 (2017).

31 Berger, A. & Loutre, M.-F. Insolation values for the climate of the last 10 million years. *Quaternary science reviews* **10**, 297-317 (1991).

32 Martin, K. C. *et al.* Greenland Ice cores reveal a south‐to‐north difference in Holocene thermal maximum timings. *Geophysical Research Letters* **51**, e2024GL111405 (2024).

33 Badgeley, J. A., Steig, E. J., Hakim, G. J. & Fudge, T. J. Greenland temperature and precipitation over the last 20 000 years using data assimilation. *Clim. Past* **16**, 1325-1346 (2020). https://doi.org:10.5194/cp-16-1325-2020

34 Miller, G. H. *et al.* Arctic amplification: can the past constrain the future? *Quaternary Science Reviews* **29**, 1779-1790 (2010). https://doi.org:https://doi.org/10.1016/j.quascirev.2010.02.008

35 Masson-Delmotte, V. *et al.* Climate change 2021: the physical science basis. *Contribution of working group I to the sixth assessment report of the intergovernmental panel on climate change* **2**, 2391 (2021).

36 Rantanen, M. *et al.* The Arctic has warmed nearly four times faster than the globe since 1979. *Communications Earth & Environment* **3**, 168 (2022). https://doi.org:10.1038/s43247-022-00498-3

37 Buylaert, J. P., Murray, A. S., Thomsen, K. J. & Jain, M. Testing the potential of an elevated temperature IRSL signal from K-feldspar. *Radiation Measurements* **44**, 560-565 (2009). https://doi.org:https://doi.org/10.1016/j.radmeas.2009.02.007

38 Galbraith, R. F., Roberts, R. G., Laslett, G. M., Yoshida, H. & Olley, J. M. Optical dating of single and multiple grains of quartz from Jinmium rock shelter, northern Australia: Part I, experimental design and statistical models. *Archaeometry* **41**, 339-364 (1999).

39 Durcan, J. A., King, G. E. & Duller, G. A. T. DRAC: Dose Rate and Age Calculator for trapped charge dating. *Quaternary Geochronology* **28**, 54-61 (2015).

40 Sohbati, R., Murray, A. S., Porat, N., Jain, M. & Avner, U. Age of a prehistoric "Rodedian" cult site constrained by sediment and rock surface luminescence dating techniques. *Quaternary Geochronology* **30**, 90-99 (2015). https://doi.org:https://doi.org/10.1016/j.quageo.2015.09.002

41 Rieckh, T., Born, A., Robinson, A., Law, R. & Gülle, G. Design and performance of ELSA v2.0: an isochronal model for ice-sheet layer tracing. *Geosci. Model Dev.* **17**, 6987-7000 (2024). https://doi.org:10.5194/gmd-17-6987-2024

42 Born, A. & Robinson, A. Modeling the Greenland englacial stratigraphy. *The Cryosphere* **15**, 4539-4556 (2021). https://doi.org:10.5194/tc-15-4539-2021

43 MacGregor, J. A. *et al.* Holocene deceleration of the Greenland Ice Sheet. *Science* **351**, 590-593 (2016). https://doi.org:10.1126/science.aab1702

44 Gkinis, V. *et al.* A 120,000-year long climate record from a NW-Greenland deep ice core at ultra-high resolution. *Scientific Data* **8**, 141 (2021).

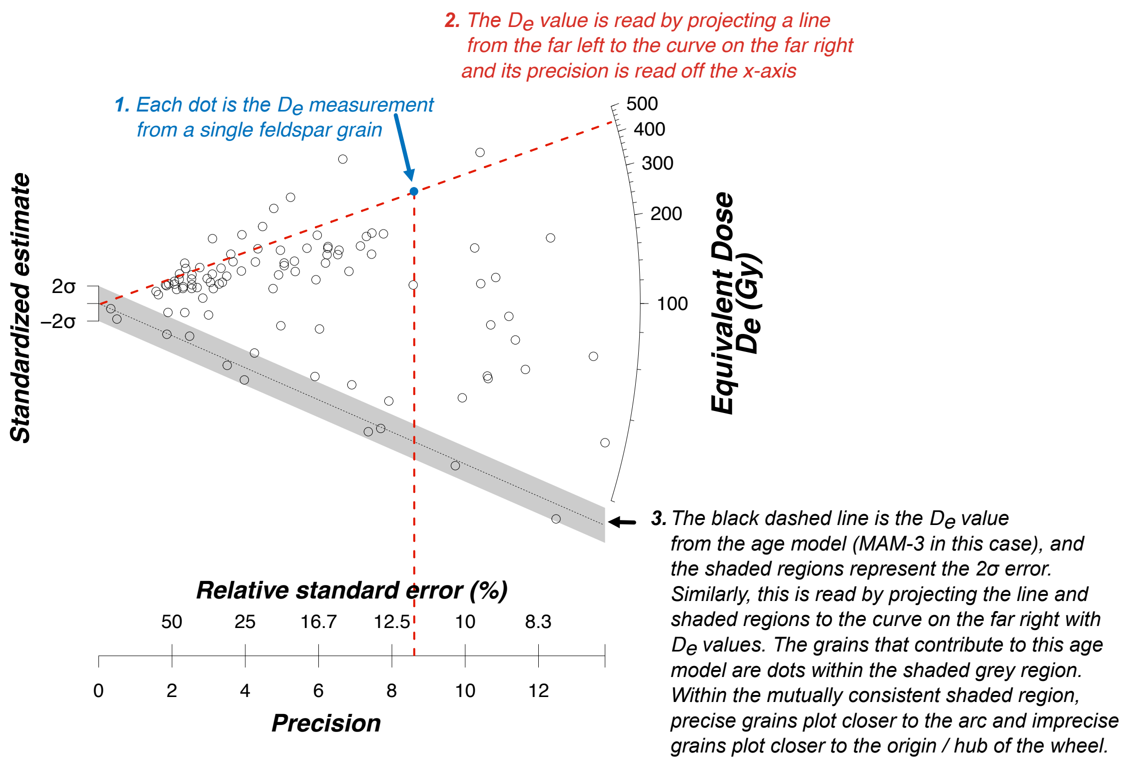

Extended Data Fig. 1. Description of how to read luminescence radial diagrams. For further information, see Galbraith (2010).

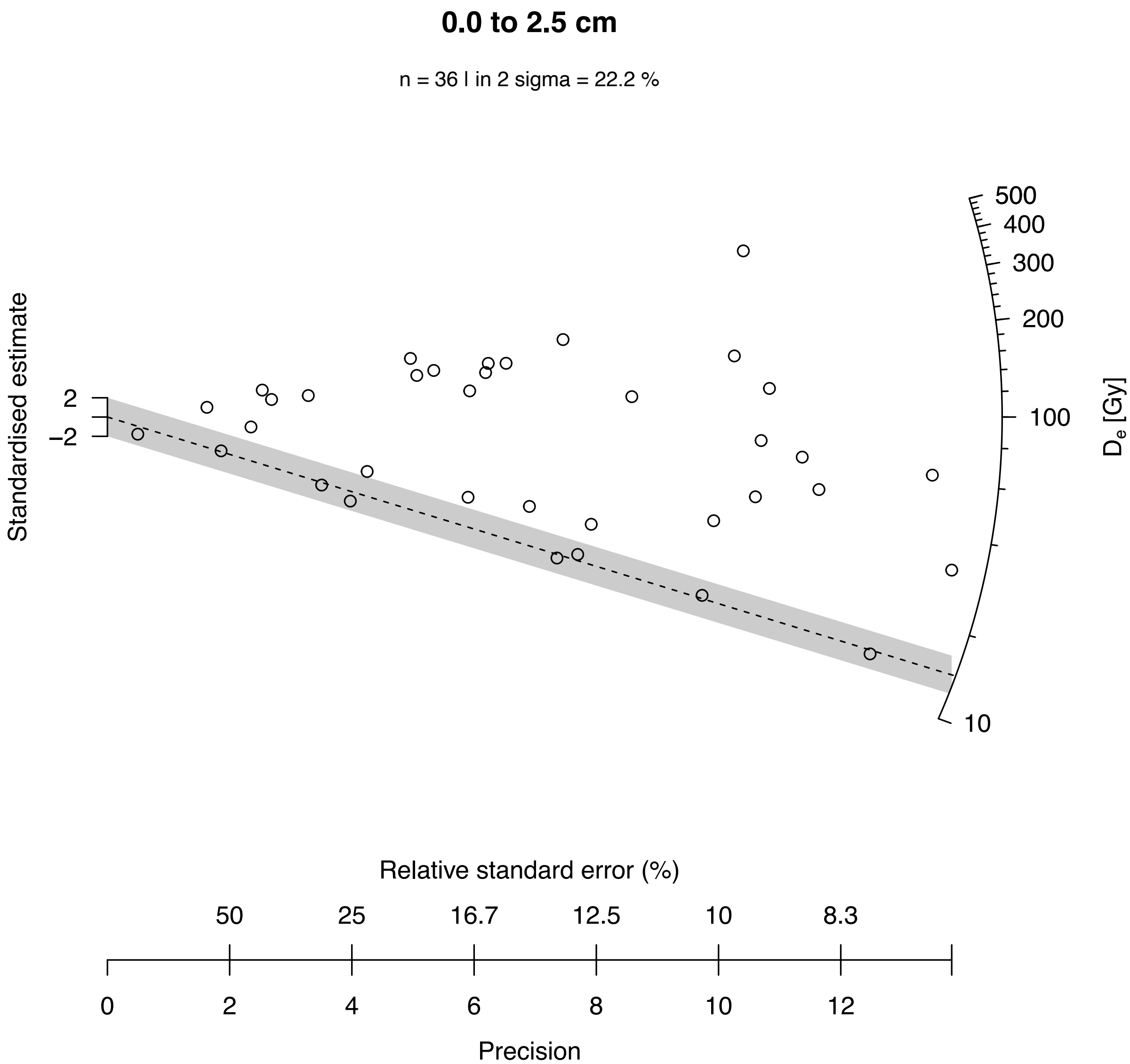

Extended Data Fig. 2. Radial plot of IRSL measurements from 0 – 2.5 cm depth.

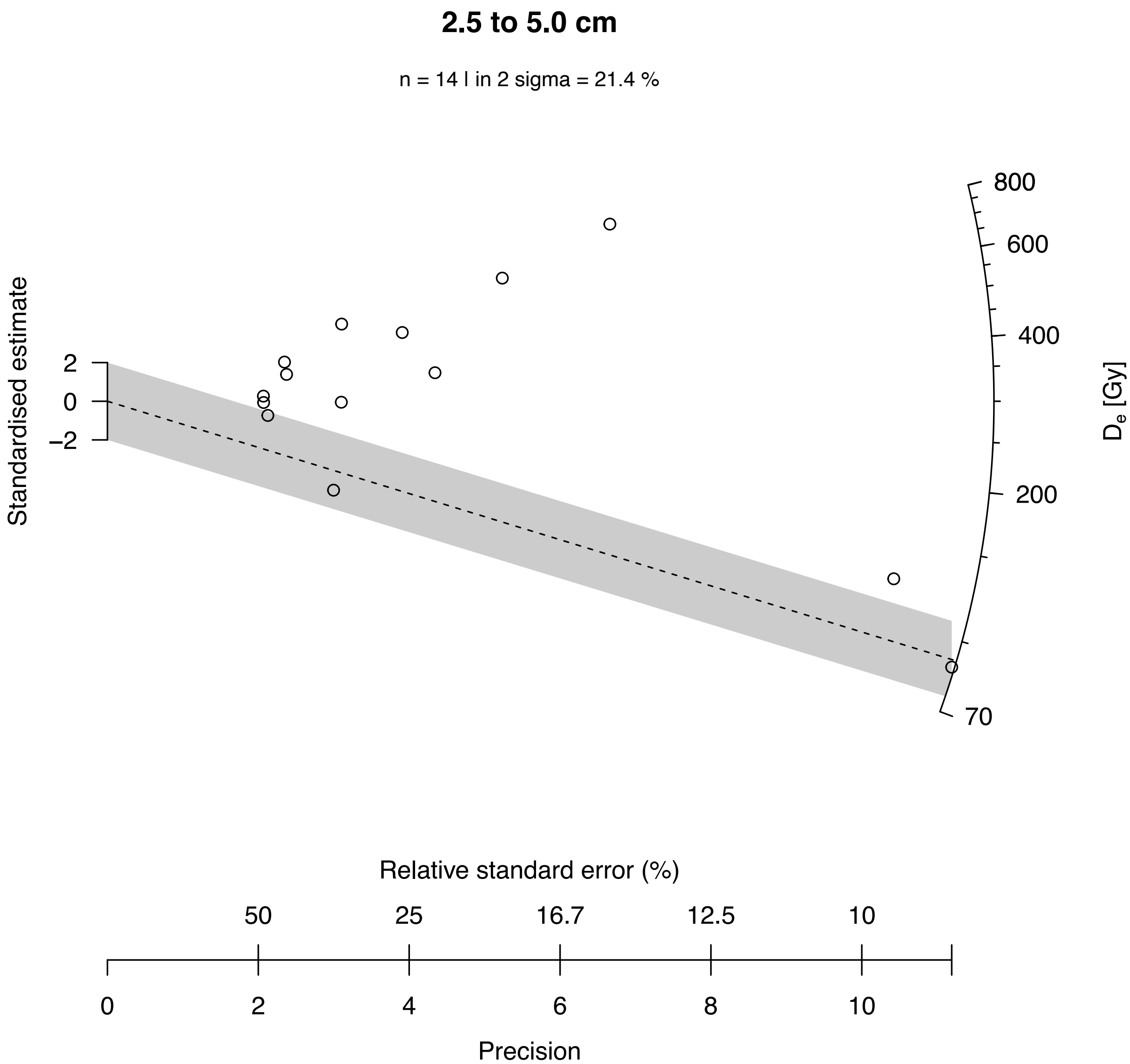

Extended Data Fig. 3. Radial plot of IRSL measurements from 2.5 – 5.0 cm depth.

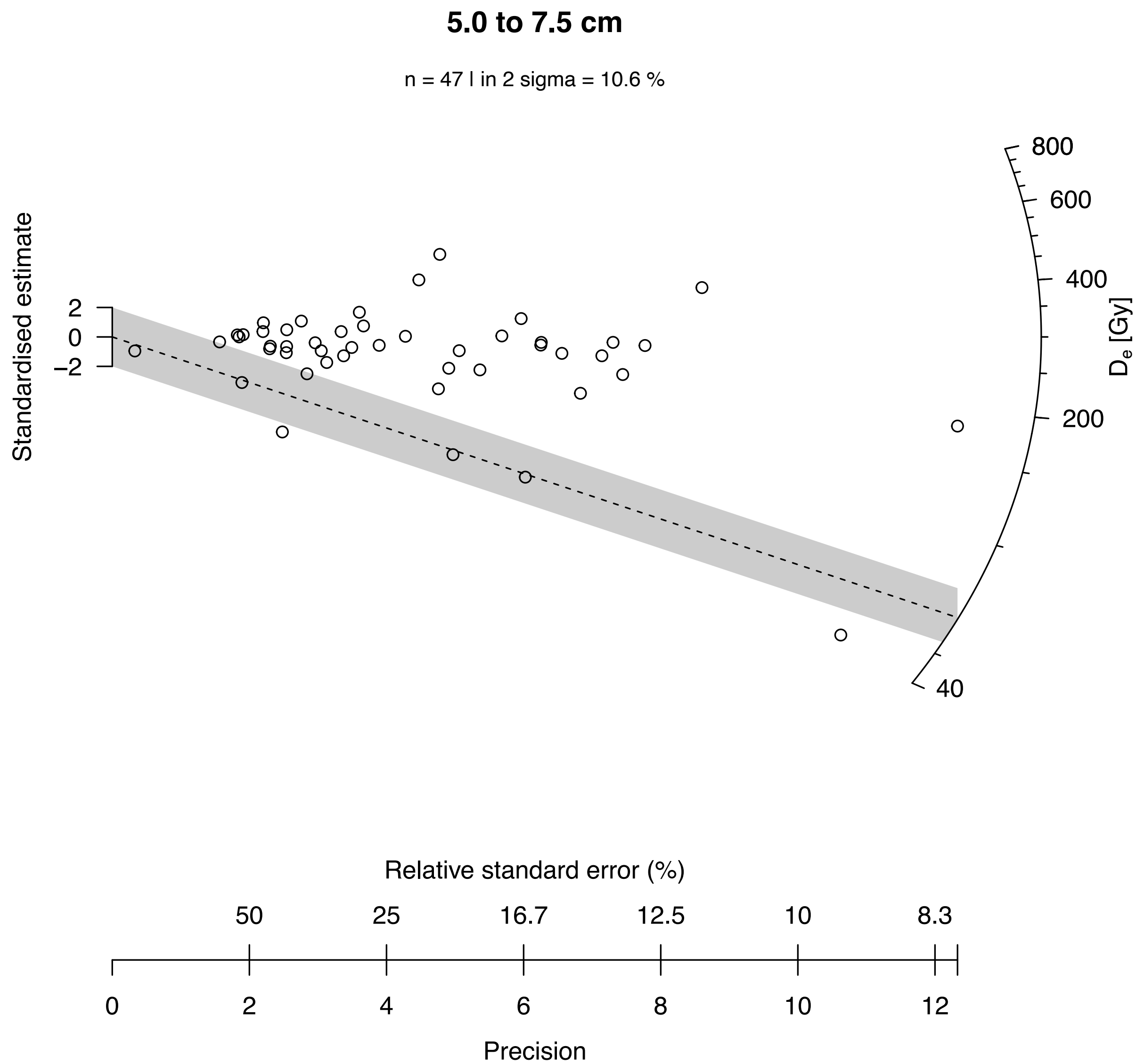

Extended Data Fig. 4. Radial plots of IRSL measurements from 5.0 – 7.5 cm depth.

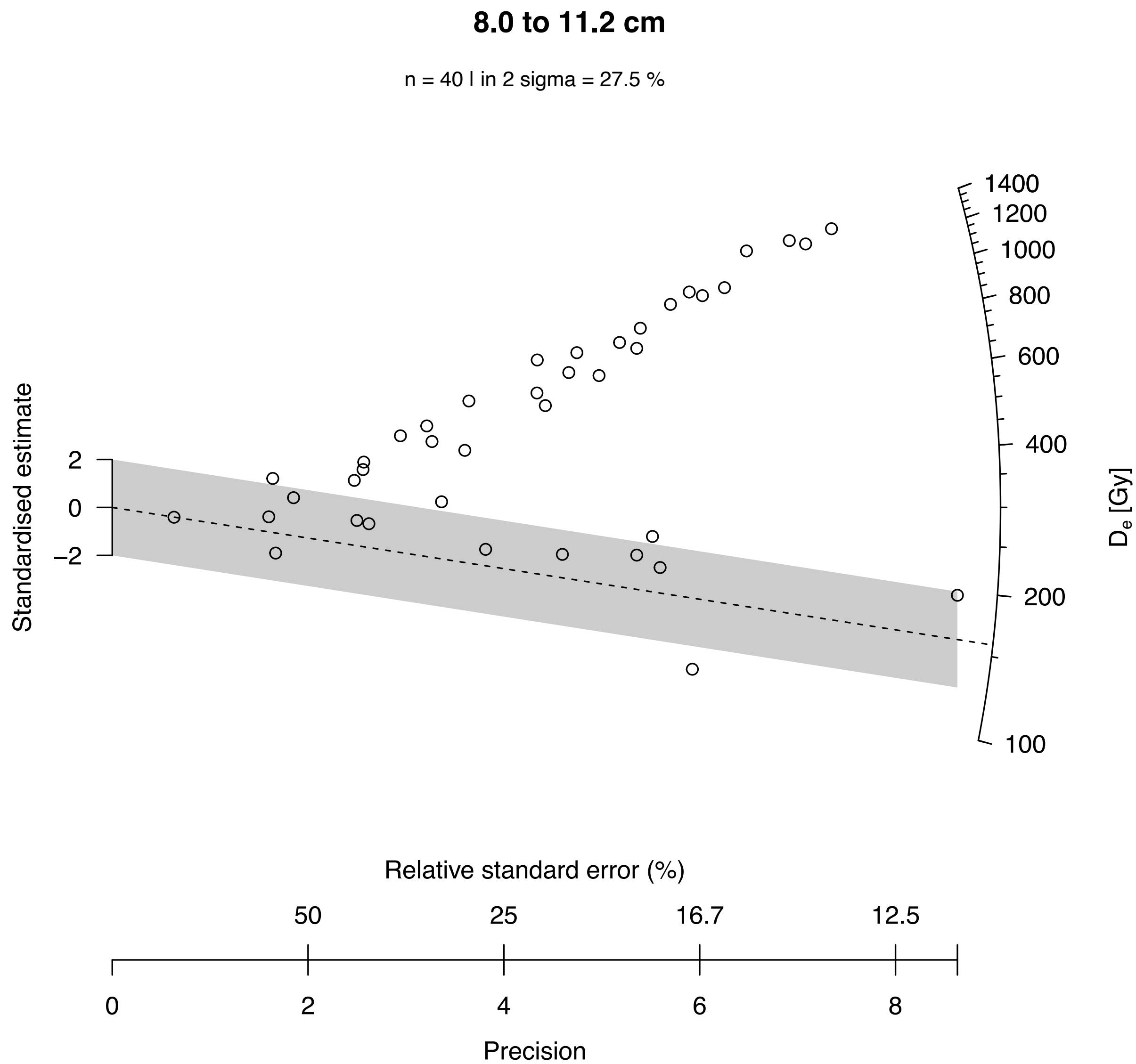

Extended Data Fig. 5. Radial plot of IRSL measurements from 8.0 – 11.2 cm depth.

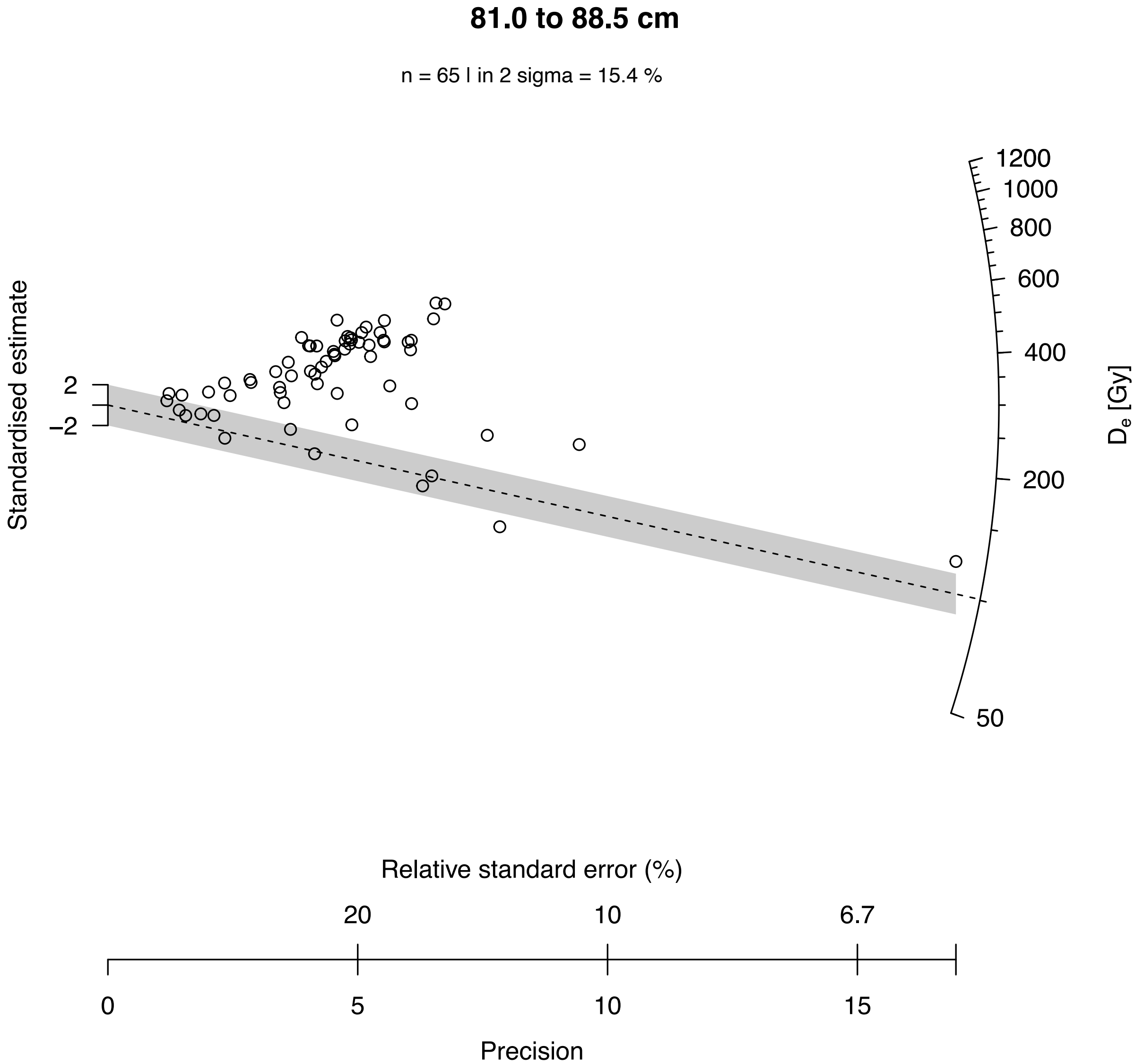

Extended Data Fig. 6. Radial plot of IRSL measurements from 81.0 to 88.5 cm depth.

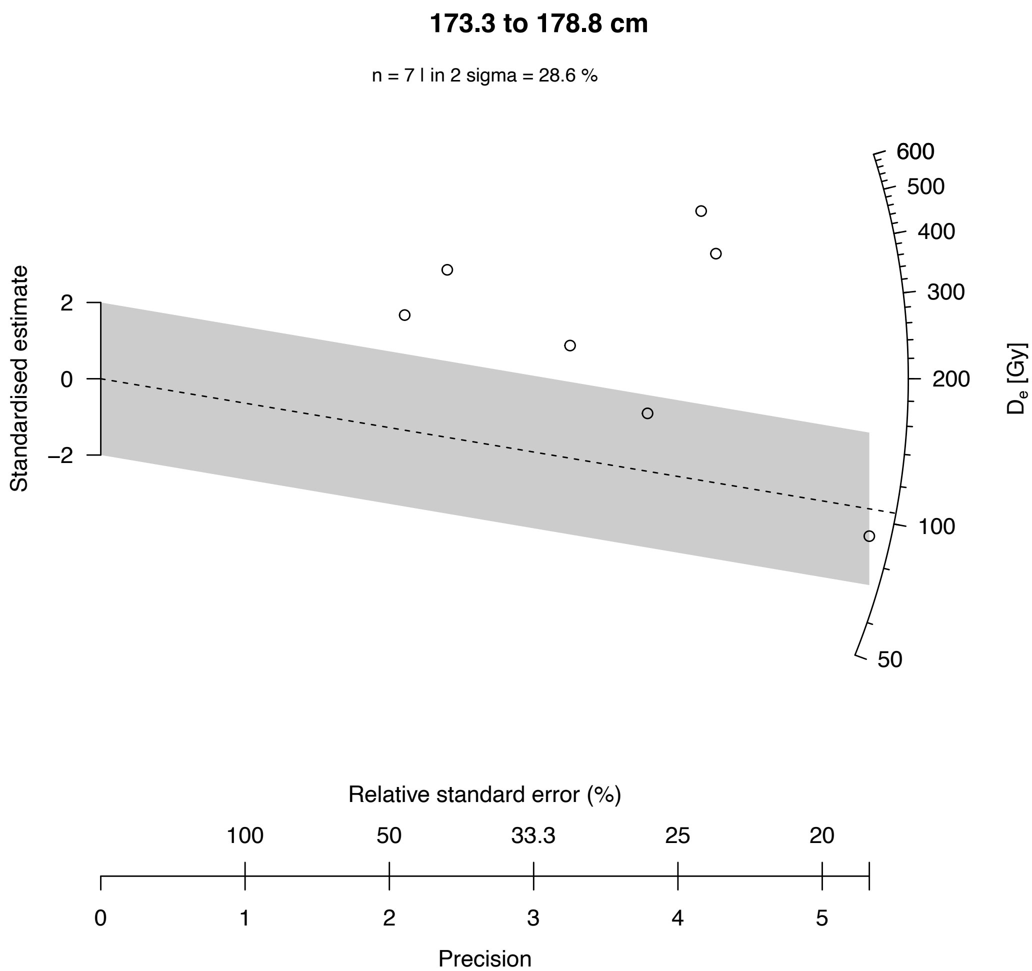

Extended Data Fig. 7. Radial plot of IRSL measurements from 173.3 to 178.8 cm depth.

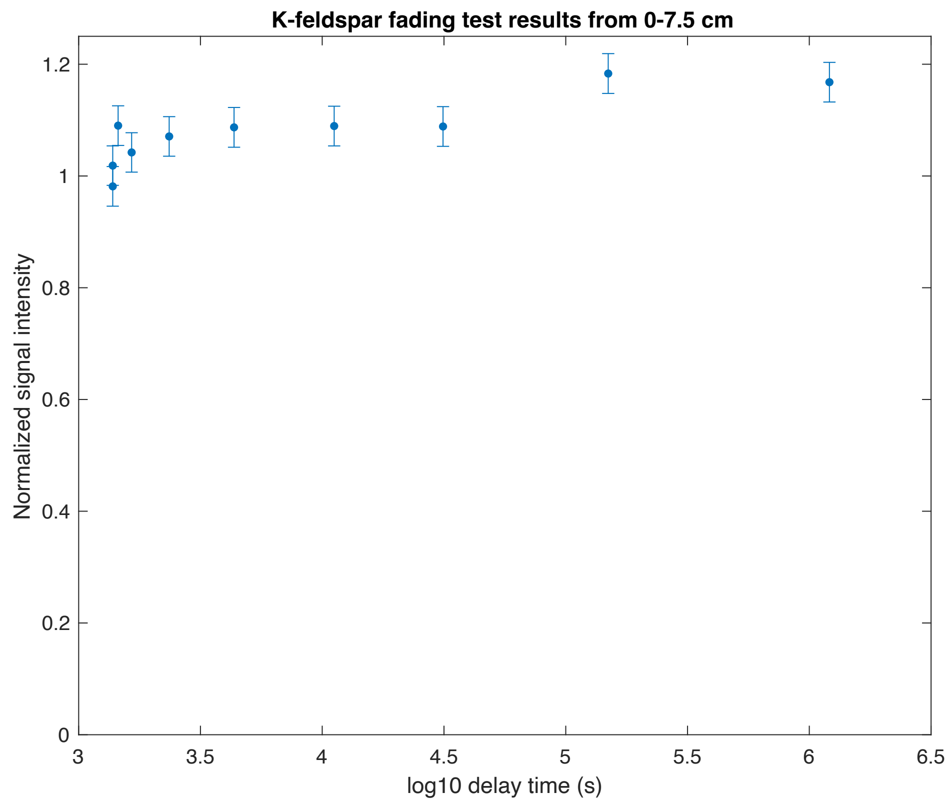

Extended Data Fig. 8. Results from K-feldspar fading tests on grains from 0 to 7.5 cm.

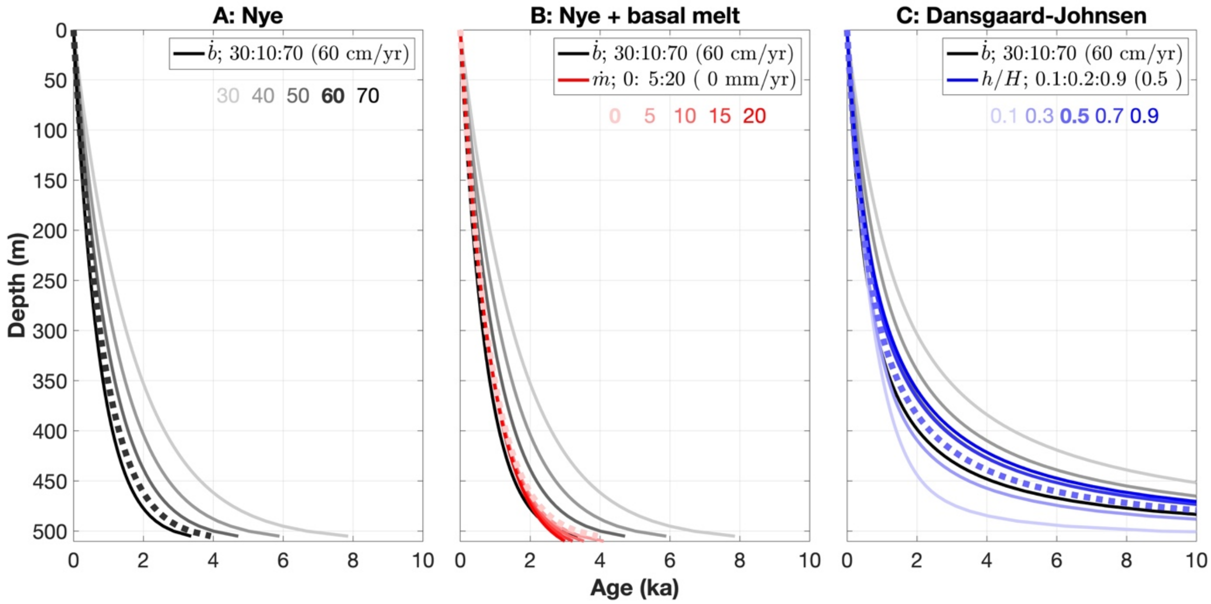

Extended Data Fig. 9. One-dimensional steady-state models of the depth–age relationship of the ice column at the Prudhoe drill site, following MacGregor et al. (2016) for model formulation. For each model parameter in each model/panel, a range of five values is considered (see legend), and the resulting depth-age relationship shown is darker for increasing values. For each model/panel, the best estimate of the modern value is shown as a thicker dashed line. A): Nye (sandwich) model depends only on accumulation rate (bdot), the ice column deforms uniformly by pure shear and is not melting at the bed. B): Nye+melt model is the same as Nye (A), except that basal melting (mdot) is included. C): Dansgaard-Johnsen model, where the ice column of thickness H deforms by pure shear above a height h above the bed, and by simple shear below it.

The first two models (Nye and Nye+melt) tend to produce younger ice columns, and regardless of parameter selection, they consistently indicate a completely Holocene ice column. The latter model (Dansgaard–Johnsen) indicates that a non-negligible basal layer of Pleistocene ice is possible at lower accumulation rates and higher basal shear layer thicknesses. From this initial modeling, we conclude that no past significant basal shear or melting is required to reproduce the measured the $\delta^{18}O$ drill ice chip record, and that simplest explanation for that record is an ice cap that regrew under a mean ice accumulation rate slightly lower than present.

REFEERENCES:

Galbraith, R. F., Roberts, R. G., Laslett, G. M., Yoshida, H., and Olley, J. M., 1999, Optical dating of single and multiple grains of quartz from Jinmium rock shelter, northern Australia: Part I, experimental design and statistical models: Archaeometry, v. 41, no. 2, p. 339-364.

MacGregor, J. A., Colgan, W. T., Fahnestock, M. A., Morlighem, M., Catania, G. A., Paden, J. D., and Gogineni, S. P., 2016, Holocene deceleration of the Greenland Ice Sheet: Science, v. 351, no. 6273, p. 590-593.